Analytica Chimica Acta 1204 (2022) 339703

Contents lists available at ScienceDirect

Analytica Chimica Acta

journal homepage: www.elsevier.com/locate/aca

N, S-co-doped carbon/$Co_{1-x}S$ nanocomposite with dual-enzyme activities for a smartphone-based colorimetric assay of total cholesterol in human serum

Jiani Li [a, b, 1], Tingting Liu [a, 1], Randy A. Dahlgren [c], Hanzhang Ye [a], Qi Wang [a], Yongli Ding [a], Ming Gao [a], Xuedong Wang [a, *], Huili Wang [b, **]

[a] Jiangsu Key Laboratory of Environmental Science and Engineering, School of Environmental Science and Engineering, Suzhou University of Science and Technology, Suzhou, 215009, China
[b] College of Laboratory Medicine and Life Sciences, Wenzhou Medical University, Wenzhou, 325035, China
[c] Department of Land, Air and Water Resources, University of California, Davis, CA, 95616, USA

HIGHLIGHTS

- N, S-co-doped carbon/$Co_{1-x}S$ nanocomposite is fabricated using a sol-gel approach.
- Nanocomposite has abundant S vacancies and Co-S nanoparticles in carbon-layer pores.
- Synergistic catalysis occurs for chromogenic reaction in NSC/$Co_{1-x}S$ nanocomposite.
- Nanocomposite has both peroxidase-like and oxidase-mimetic dual-enzyme activities.
- A "Thing Identify" application offers low detection limit for cholesterol in serum.

GRAPHICAL ABSTRACT

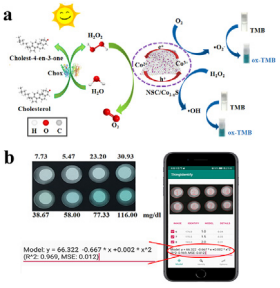

ARTICLE INFO

Article history:
Received 7 November 2021
Received in revised form
11 February 2022
Accepted 7 March 2022

Keywords:
N
S co-doped carbon/$Co_{1-x}S$ nanomaterials
Dual-enzyme activity
Smartphone "Thing identify" app
Colorimetric sensor
Cholesterol

ABSTRACT

We fabricated a novel N,S-co-doped carbon/$Co_{1-x}S$ nanocomposite (NSC/$Co_{1-x}S$) using a facile sol-gel approach, which featured a multiporous structure, abundant S vacancies and Co-S nanoparticles filling the carbon-layer pores. When the $Co_{1-x}S$ nanoparticles were anchored onto the surface of N,S-co-doped carbon, a synergistic catalysis action occurred. The NSC/$Co_{1-x}S$ nanocomposites possessed both peroxidase-like and oxidase-mimetic dual-enzyme activities, in which the oxidase-mimetic activity dominated. By scavenger capture tests, the nanozyme was demonstrated to catalyze H_2O_2 to produce h^+, •OH and $•O_2^-$, among which the strongest and weakest signals were h^+ and •OH, respectively. The multivalence states of Co atoms in the NSC/$Co_{1-x}S$ structure facilitated electronic transfer that enhanced redox reactions, thereby improving the resultant color reaction. Based on the NSC/$Co_{1-x}S$'s enzyme-mimetic catalytic reaction, a visual colorimetric assay and Android "Thing Identify" application (app), installed on a smartphone, offered detection limits of 1.93 and 2.51 mg/dl, respectively, in human serum samples. The selectivity/interference experiments, using fortified macromolecules and metal ions, demonstrated that this sensor had high selectivity and low interference potential for cholesterol analysis. Compared to standard assay kits and previously reported visual detection, the Android smartphone-based assays

* Corresponding author.
** Corresponding author.
E-mail addresses: zjuwxd@163.com (X. Wang), whuili@163.com (H. Wang).
[1] Tingting Liu and Jiani Li are the co-first author.

https://doi.org/10.1016/j.aca.2022.339703

provided higher accuracy (recoveries up to 93.6−104.1%), feasibility for trace-level detection, and more convenient on-site application for cholesterol assay due to the superior enzymatic activity of NSC/$Co_{1-x}S$. These compelling performance metrics lead us to posit that the NSC/$Co_{1-x}S$-based nanozymic sensor offers a promising methodology for several practical applications, such as point-of-care diagnosis and workplace health evaluations.

1. Introduction

Physical health refers to the state of well-developed organ systems, normal physiological functions, healthy physique, proper metabolism and good work efficiency [1]. It is usually measured by physical measurements, body examinations and various physiological indicators. Therefore, real-time body monitoring technology is very important for assessing and maintaining physical health. Total cholesterol is an important indicator of physical health associated with the synthesis of vitamin D, bile acids and steroid hormones. An optimum total cholesterol range in serum from a healthy adult is 112.13−231.99 mg/dl [2]. If cholesterol levels are too high, it will induce fatty liver, coronary heart disease, myocardial infarction, strokes, etc. On the contrary, abnormally low cholesterol levels may increase the risk of hemorrhagic stroke and colon cancer [2,3]. Therefore, early detection of abnormal total cholesterol concentration in serum has a profound impact on point-of-care diagnosis applications.

Current clinical methods for monitoring total cholesterol use a fully automatic biochemical analysis instrument, which imposes several disadvantages for routine/low cost monitoring, such as a high instrument purchase cost, maintenance of a technical analytical instrument, and the potential for cross-contamination. Thus, there is a prominent need for developing a technique for total cholesterol monitoring of human serum that is simple, rapid, accurate and achieved at a low price. Several, methodologies are available for the assay of cholesterol in serum, including chromatography analysis [4], colorimetric methods [5,6], electrochemiluminescence methods [6,7], fluorescence detection [8,9], and electrochemical analysis [10,11]. Among these approaches, colorimetric methods have garnered considerable attention due to their simple, visually observable and convenience protocols. Erickson's group (2014) developed smartphone accessories and software application, and successfully realized the visual detection of total cholesterol in human blood, which solved the puzzles of high cost, complex operation, and difficulty in convenient storage and processing of the test results for the traditional test-paper method [12]. It could accurately quantify the total cholesterol level in blood within 60 s through imaging standard test strips, but was only satisfactory in the physiological concentration range (140−400 mg/dl), and not feasible for the trace-level detection of cholesterol. Tan et al. (2020) prepared a portable cholesterol assay kit by coupling the peroxidase-like activity of polypyrrole nanoparticles (PPy NPs) and cholesterol oxidase (ChOx), which realized the on-site semi-quantitative and visual detection of cholesterol in human serum by virtue of forming agarose gel; it offered the linear range of 0.39−3.87 mg/dl, detection limit of 0.14 mg/dl and relative recoveries of 96.0−106.9% for total cholesterol [13]. Gao and coworkers (2007) reported on the use of Fe_3O_4 magnetic nanoparticles (MNPs) with peroxidase-like activity to successfully constructed a colorimetric method based on a nanoenzyme [14]. In the presence of H_2O_2, the Fe_3O_4 MNPs catalyze the chromogenic substrate 3,3′,5,5′-tetramethylbenzidine (TMB) to 3,3′,5,5′-tetramethyldiphenone (TMBox), which develops a maximum absorbance at 652 nm. The development of such H_2O_2-based sensors has broad application prospects in the fields of environmental chemistry, biotechnology and medicine. A variety of nanomaterials, such as metal oxides [15], carbon-based nanomaterials [16,17] and metal sulfides [15,18,19], have been reported to develop peroxidase-like activity. Among them, carbon materials have the advantages of stable properties, wide application and simple preparation. For example, Zhang and colleagues (2020) fabricated carbon dots for ratiometric and colorimetric detection of Cu^{2+} [20]. Further, Wang et al. (2021) developed a full-wavelength coverage (blue to red) colorimetric sensor based on polymer-carbon nanodots for visual detection of nitrite via a smartphone APP [21]. Moreover, Nattasa et al. (2021) reported mimicking peroxidase-like activity of nitrogen-doped carbon dots (N-CDs) coupled with a laminated three-dimensional microfluidic paper-based analytical device (laminated 3D-μPAD) for smart sensing of total cholesterol from whole blood [22]. However, these carbon-based materials have several shortcomings, such as susceptibility to aggregation, high detection limit, small linear range and low color sensitivity, which limit their potential applications.

Recent research has focused on using a variety of strategies to modify carbon-based materials to alleviate some of the analytical limitations associated with carbon-based materials. These alteration strategies include heat treatment [23], acid treatment [24] and doping [25,26], of which metal compound doping (metal oxides and metal sulfides) holds great potential. Anaclet et al. (2019) developed a multifunctional magnetic Fe_3O_4/nitrogen-doped porous carbon nanocomposite for removal of dyes and sensing applications [27]. Further, the adsorption and redox conversion behaviors of Cr(VI) were analyzed in detail on goethite/carbon microspheres and akaganeite/carbon microsphere composites [28]. Finally, a Co_9S_8/CoS@S,N co-doped porous carbon derived from MOFs was confirmed to be an efficient catalyst for the oxygen evolution reaction [29]. In contrast to metal oxides, metal sulfides have the advantages of not being easily oxidized, strong stability and good electrical conductivity, which lead us to select carbon-based materials doped with metal sulfides as the focus of this investigation.

Several studies have examined the properties and use of iron sulfide, copper sulfide and cobalt sulfide-based nanozymes. For instance, Ding and colleagues (2020) reported a hybrid FeS_2 nanoparticle encapsulated by two-dimensional carbon sheets for use as a nanozyme for colorimetric glucose assay (LOD = 0.0074 mg/dl) [30]. Further, Farzin and coworkers (2018) synthesized a highly ordered 3D flower-like hierarchical CuS hollow nanosphere@N-S-rGO bionanocomposite for glucose detection. This material provided a remarkable enhancement (~40-fold) in the glucose detection limit that was attributed to rapid electron transfer on the surface of the 3D CuS NSs@N-S-rGO and the synergistic interaction of 3D CuS NSs and N-S-rGO [31]. Moreover, a colorimetric ascorbic acid sensor was developed based on a synergistic catalytic strategy using 5,10,15,20-tetra (4-pyridyl) −21H, 23H-porphyrin functionalized CuS nanohexahedrons that enhanced peroxidase-like activity [32]. Two-dimensional porphyrin-Co_9S_8 nanocomposites were confirmed to

possess synergistic peroxidase-like catalysis leading to utilization in colorimetric biosensing of H_2O_2 and glutathione with a detection limit of 0.0075 mg/dl [33]. Compared to Fe-S and Cu-S metal compounds, there is a paucity of information regarding the properties of Co-S compounds and their potential for use in environment and human-health applications.

Building upon previous studies, we developed a novel N, S-co-doped nanocomposite by employing carbon-based nanomaterials and Co-S chemicals for preparation of a highly efficient nanozyme. Two mimic enzymes, N, S-co-doped carbon (NSC) and NSC/$Co_{1-x}S$ nanocomposites, were fabricated and their differential enzymatic activities were analyzed in detail. The as-constructed NSC/$Co_{1-x}S$ mimic enzyme was further applied to develop a total cholesterol assay for human serum. A series of characterization techniques were employed to identify the morphologies and physicochemical characteristics of the synthesized nanocomposites. Based on the favorable enzyme-like mimic activity of the NSC/$Co_{1-x}S$ nanomaterial, a colorimetric biosensing platform was established to monitor total cholesterol in human serum. The operational procedure was optimized using the one-factor-at-a-time approach for incubation temperature, solution pH and material dosage. Finally, an Android "Thing Identify" app installed on a smartphone was designed and employed for real-time assay of serum cholesterol.

2. Experimental section

2.1. Chemical reagents

A series of regents with analytical or chromatographic grade were purchased from Adams (Shanghai, China): sodium alginate (SA), trithiocyanuric acid (TA), citric acid (CA), cobalt(II) acetate tetrahydrate, hydrogen peroxide (H_2O_2, 30%), acetic acid (CH_3COOH, ≥98.0%), sodium acetate (CH_3COONa, ≥99.0%), ethanol (≥99.7%), dimethyl sulfoxide (DMSO, ≥99.0%), p-benzoquinone (PBQ), ethylenediamine tetraacetic acid (EDTA), sucrose (Suc), D-histidine (His), galactose (Gal), and D-serine (Ser). Isopropyl alcohol (IPA, ≥99.5%) was gratis supplied by Greagent (Shanghai). Cholesterol (Cho, >95.0%) and 3,3′,5,5′-Tetramethyl benzidine (TMB) were obtained from Aladdin (Shanghai). Cholesterol lipase (Chol, ≥300 units/g) was acquired from Rhawn (Shanghai) and cholesterol oxidase (Chox) from Macklin (Shanghai). All reagents were used when received without further purification. Ultrapure water (>18.2 MΩ) was generated with a Milli-Q Gradient system (Bedford, MA, USA).

2.2. Synthesis of N, S-co-doped carbon (NSC)

Firstly, 5.0 g of TA, 1.0 g of SA and 0.5 g of CA were added to 99 mL of deionized water, and the solution was magnetically stirred for 12 h to form a homogeneous phase at room temperature. This mixture was dehydrated by freeze-drying to form an aerogel. Subsequently, the as-prepared aerogel was transferred into a quartz boat and placed in a tube furnace; the air in the furnace was exhausted using a gentle N_2 flow for ~20 min. Next, the quartz boat was heated under the protection of N_2 at a rate of 2 °C/min to 500 °C and kept for 30 min, then heated again at a rate of 5 °C/min to 700 °C and kept for 120 min. After the tube furnace was cooled to room temperature, the calcined aerogel was collected and washed/rinsed three times with Milli-Q ultrapure water. Finally, the resultant light yellow product, hereafter referred to as NSC, was dried at 60 °C for 6 h in a vacuum oven.

2.3. Synthesis of NSC/$Co_{1-x}S$ nanocomposite

Briefly, 5.0 g of TA, 1.0 g of SA and 0.5 g of CA were dissolved in 99 mL of deionized water and magnetically stirred for 12 h to acquire a homogeneous solution (A) at ambient conditions. Subsequently, 0.5 g of $Ni(CH_3COO)_2{\cdot}4H_2O$ was dissolved in 100 mL of deionized water to prepare solution B. Solution B was slowly added to solution A, and the resultant mixed solution was magnetically stirred for 12 h to form a homogeneous phase. Then, the material was subjected to the same freeze drying, heating and washing procedures listed above for the synthesis of NSC. The final product was designated as NSC/$Co_{1-x}S$ nanocomposite (Fig. 1.). To obtain an individual $Co_{1-x}S$ product, TA, CA and cobalt acetate tetrahydrate (without addition of SA) were magnetically stirred for 6 h, and subsequently the mixture was centrifuged and lyophilized (Fig. S1).

2.4. Characterization of NSC and NSC/$Co_{1-x}S$ nanocomposites

The morphologies and elemental mapping of NSC and NSC/$Co_{1-x}S$ were acquired using field emission scanning electron microscopy and energy dispersive X-ray (FESEM, QUANTA FEG; EDS, Oxford) and transmission electron microscopy (TEM, FEI Tecnai F20). X-ray diffraction (XRD, D8-Advance, Bruker) was used to determine the crystalline structure of samples. X-ray photoelectron spectroscopy (XPS) was performed using a Thermo Scientific K-Alpha Instrument. Brunauer-Emmett-Teller (BET) surface area and pore-size distribution curves were recorded on a MicroActive for TriStar II Plus Instrument. Raman analysis was accomplished using an Invia Reflex, LabRam HR Evolution Instrument. Enzyme kinetics and UV−vis spectra were carried out on a UV-5500PC spectrophotometer (Metash). A Bruker EMXPLUS was used to measure S vacancies and free radicals.

2.5. Enzymatic activity of the NSC/$Co_{1-x}S$ nanocomposite

Upon reaction of NSC/$Co_{1-x}S$ with H_2O_2, the catalytic oxidation of TMB was measured using an ultraviolet spectrophotometer. Briefly, 60 μL of 1 mg/mL NSC/$Co_{1-x}S$ suspension was added to 1700 μL of NaAc-HAc buffer solution (20 mM, pH = 3.6). Then, 200 μL of 6 mM TMB and 40 μL of 50 mM H_2O_2 were sequentially added to the above solution. After incubation at 50 °C for 20 min and filtering through a 0.45-μm cellulose mixture filter, the 652-nm absorbance of the resultant solution was recorded.

Steady-state kinetic analysis of TMB by NSC/$Co_{1-x}S$ was performed using the conditions described above, but with varying initial concentrations of TMB (0.01, 0.025, 0.05, 0.1, 0.25, 0.5, 0.75, 1.0, 1.5 and 2.0 mM). For the kinetic analysis using H_2O_2 as a substrate, a series of initial H_2O_2 levels (0.1, 0.3, 0.5, 0.8, 1.0, 2.0, 3.0, 4.0, 5.0, 6.0, 7.0, 8.0, 9.0, 10.0 and 15.0 mM) were utilized with a constant TMB concentration of 6 mM. The 652-nm optical density (OD) was measured on a UV-5500PC Spectrophotometer. By fitting the time-scanning OD data in the Michaelis-Menten equation, the catalytic parameters for the steady-state kinetic analysis were obtained. The Michaelis-Menten equation **(1)** describes the relationship between the conversion rate of a given substrate and the substrate concentration of an enzyme (NSC/$Co_{1-x}S$ in this case):

$$\frac{1}{V} = \left(\frac{K_m}{V_{max}}\right) * \left(\frac{1}{[S]}\right) + \frac{1}{V_{max}} \quad (1)$$

where K_m is the Michaelis constant, V_{max} is maximum reaction velocity and *[S]* is TMB concentration.

2.6. Capture test for reactive oxygen species (ROS)

Previous studies demonstrated the scavenging abilities of isopropyl alcohol (IPA), ethylenediamine tetraacetic acid (EDTA) and *p*-benzoquinone (PBQ) for hydroxyl radicals (·OH), electron holes (h^+) and superoxide radicals ($\cdot O_2^-$), respectively [5,34]. To

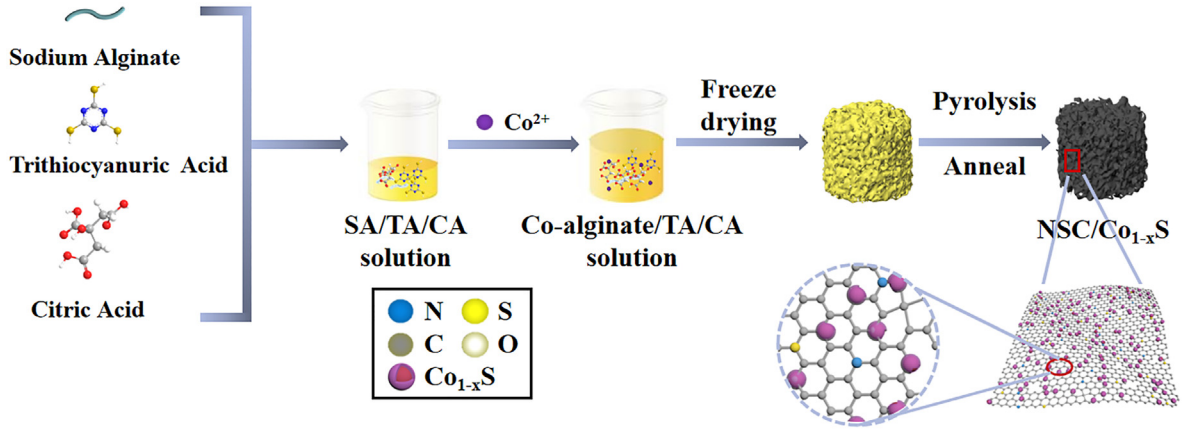

Fig. 1. Schematic diagram of the NSC/$Co_{1-x}S$ synthesis process.

investigate which species of ROS participate in the catalytic reaction, we independently added 200 μL of each scavenger and 100 μL of the NSC/$Co_{1-x}S$ nanocomposite solution to the 2 mL H_2O_2-TMB system, and subsequently measured the 652-nm ODs after a 20min incubation after filtering through a 0.45-μm cellulose mixture filter. On the basis of changes in the Michaelis constant (K_m), we determined the most prominent ROS species promoting the enzymatic reaction.

2.7. Colorimetric detection of cholesterol

A cholesterol calibration curve was generated using 100 μL of cholesterol (7.73–386.65 mg/dl), 50 μL cholesterol esterase (1 mg/mL) and 50 μL of cholesterol oxidase (2 mg/mL) reacting with 50 μL of PBS buffer (20 mM, pH = 7) at 37 °C for 30 min. The reacted solution was then added to a mixture containing 200 μL of TMB (6 mM), 60 μL of NSC/$Co_{1-x}S$ (1 mg/mL) and 1490 μL of NaAc-HAc buffer solution (20 mM, pH = 3.6). After a 20-min incubation at 50 °C and filtering through a 0.45-μm cellulose mixture filter, the 652-nm absorbance of the resultant solution was recorded.

To explore potential interference effects in the cholesterol detection procedure, various macromolecules and ions were independently fortified at a 10.0 mM concentration: galactose (Gal), sucrose (Suc), glucose (Glu), D-histidine (His), D-serine (Ser), NaCl, KCl and $MgSO_4$. In this interference assessment, the cholesterol concentration was held constant at 1.0 mM. The subsequent cholesterol measurement procedure was the same as described above.

To investigate the reproducibility of NSC/$Co_{1-x}S$ nanocomposites for cholesterol detection, the reaction solution after a 20-min incubation at 50 °C was centrifuged at 5000 rpm for 3 min. The 652-nm ODs of the resultant supernatant were measured using a UV–vis spectrometer. The filtered NSC/$Co_{1-x}S$ nanocomposites were washed and dried for the next-round colorimetric assay as described above.

2.8. Assay of total cholesterol in human serum samples

Human serum samples (6 samples) were provided by the Henan Huaiyang People's Hospital (Huaiyang, China) and stored at −80 °C prior to use. Before assay, the frozen serum samples were thawed at 4 °C, and then centrifuged at 10,000 rpm for 20 min to remove any large agglomerates. The supernatant was diluted 10 fold with PBS buffer (20 mM, pH = 7.0) to obtain the pretreated serum sample. An aliquot (100 μL) of the pretreated serum sample, 50 μL of cholesterol esterase (1 mg/mL) and 50 μL of cholesterol oxidase (2 mg/mL) were mixed in 50 μL of PBS buffer (20 mM, pH = 7), and then incubated at 37 °C for 30 min. The subsequent assay procedures followed the aforementioned cholesterol detection.

2.9. Smartphone application for total cholesterol assay

An Android smartphone application (APP) based on the NSC/$Co_{1-x}S$ colorimetric sensor was developed for use as a blood cholesterol assay. The "Thing Identify" app was designed in 2018 by our group[36], and can be downloaded at http://iwater.wmu.edu.cn/info/1042/1191.htm; the operational procedures are described in detail within the app. When selecting the "Thing Identify" icon, a new page appears, in which there are four option buttons: "IMAGE", "IDENTIFY", "MODEL" and "DETAILS" (Fig. 2a). When the "IMAGE" button is selected, two icons of "Capture" and "Gallery" appear (Fig. 2b). The target image can be selected from the available images containing the blue reaction solutions representing different cholesterol concentrations (Fig. 2c). At the bottom of the main screen, a new page will appear when you select the "Options" button. The user can select "linear regression" or "polynomial regression" as the calibration option from this page, and also adjust the parameters for image recognition (Fig. 2d). Selecting the "MODEL" button will return to the main screen, where the user can then select the "IDENTIFY" button, and the app will automatically measure the color intensity in the image (Fig. 2e). By adjusting "param1" and "param2", the software will recognize all target colors, but not any non-target colors. When you enter the corresponding concentration of each sample and select "MODEL", a standard curve of cholesterol concentration versus target color (grayscale) will be generated (Fig. 2f). After the calculation is complete, you will select the "Identify" button at the bottom of the screen to open a new page (Fig. 2g). Subsequently, the "IMAGE" button can be selected to choose the test sample picture. Finally, by selecting "IDENTIFY", the screen will display the corresponding gray-scale value and its corresponding cholesterol concentration (Fig. 2h).

3. Results and discussion

3.1. Synthesis and characterization of NSC/$Co_{1-x}S$ nanocomposite

The SEM images of NSC exhibited a smooth surface and porous surface structure (Fig. 3a). After affixing NSC with $Co_{1-x}S$ nanomaterials, some small particles were observed to adhere to the surface of the porous carbon layer (Fig. 3b). Based on TEM images of NSC/$Co_{1-x}S$, many $Co_{1-x}S$ nanoparticles were homogeneously

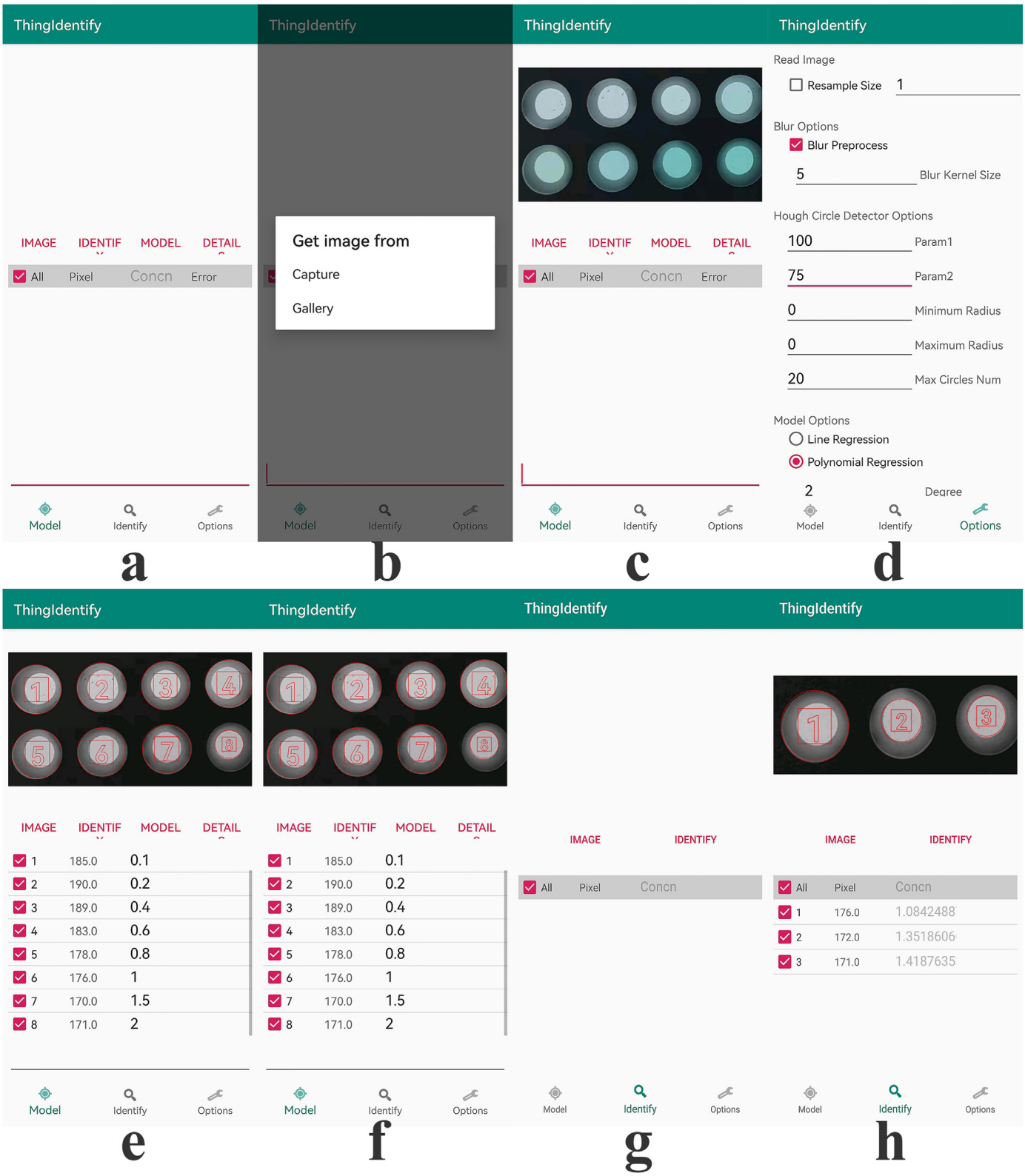

Fig. 2. The procedures of smartphone-based device for cholesterol quantification.

dispersed on the carbon layer, and had a diameter of ~10–20 nm (Fig. 3c). In the HRTEM images, we observed distinct lattice fringes with a spacing of ~0.29 nm assigned to the (102) crystallographic axis of $Co_{1-x}S$ (Fig. 3d) and ~0.34 nm assigned to the (002) crystallographic axis of C. Notably, no cobalt-sulfur compound was formed by the synthesis procedure as demonstrated by the lack of cobalt in the EDS spectrum (Fig. S2). The mass percentages of C, N, Co and S were 47.6%, 37.8%, 11.8% and 2.9%, respectively, in the EDS

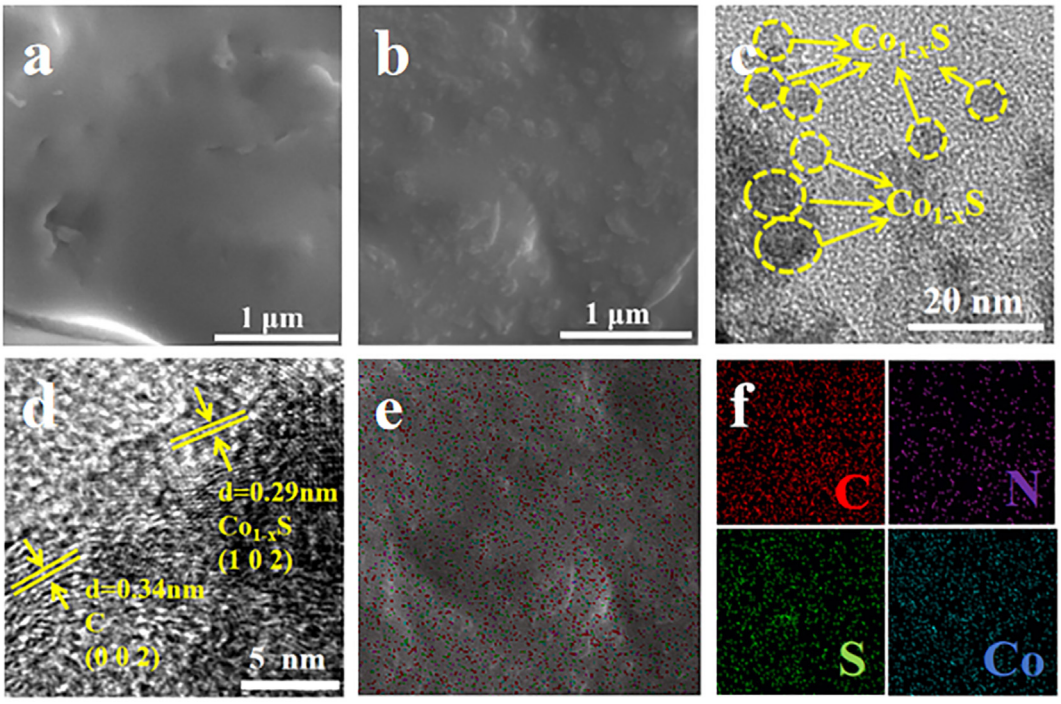

Fig. 3. (a, b) SEM images of NSC and NSC/$Co_{1-x}S$, respectively; (c) TEM image; (d) HRTEM image; and (e, f) Elemental mappings of NSC/$Co_{1-x}S$.

spectra of the NSC/$Co_{1-x}S$ nanocomposite (Fig. S3). Further, the EDS elemental mapping demonstrates that Co, N and S atoms were co-doped in the carbon layers (Fig. 3e and f).

XRD was used to assess the phase purity and crystallinity of the NSC/$Co_{1-x}S$ nanocomposite (Fig. 4a). The wide diffraction peak spanning the range of 20–30° was indexed to amorphous carbon

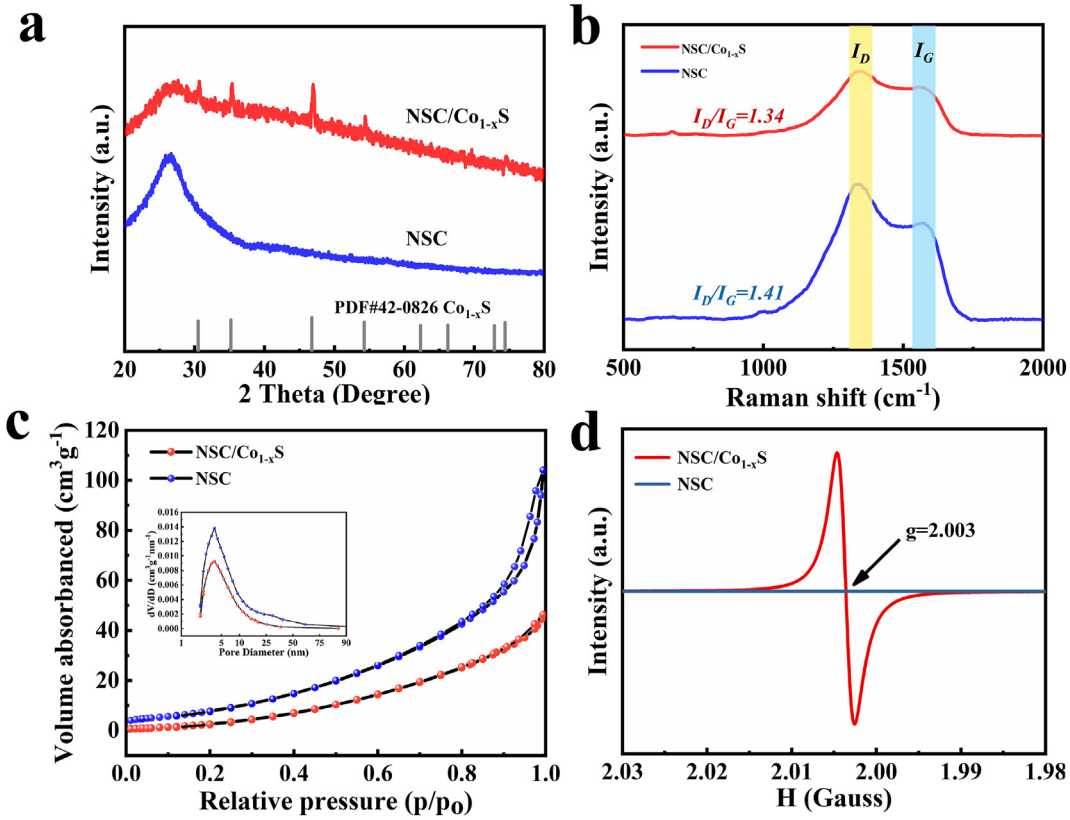

Fig. 4. Characterization of the NSC and NSC/$Co_{1-x}S$. (a) XRD patterns; (b) Raman spectra; (c) Nitrogen adsorption-desorption isotherms and pore size distribution curves (insert images); and (d) Electron spin resonance spectra.

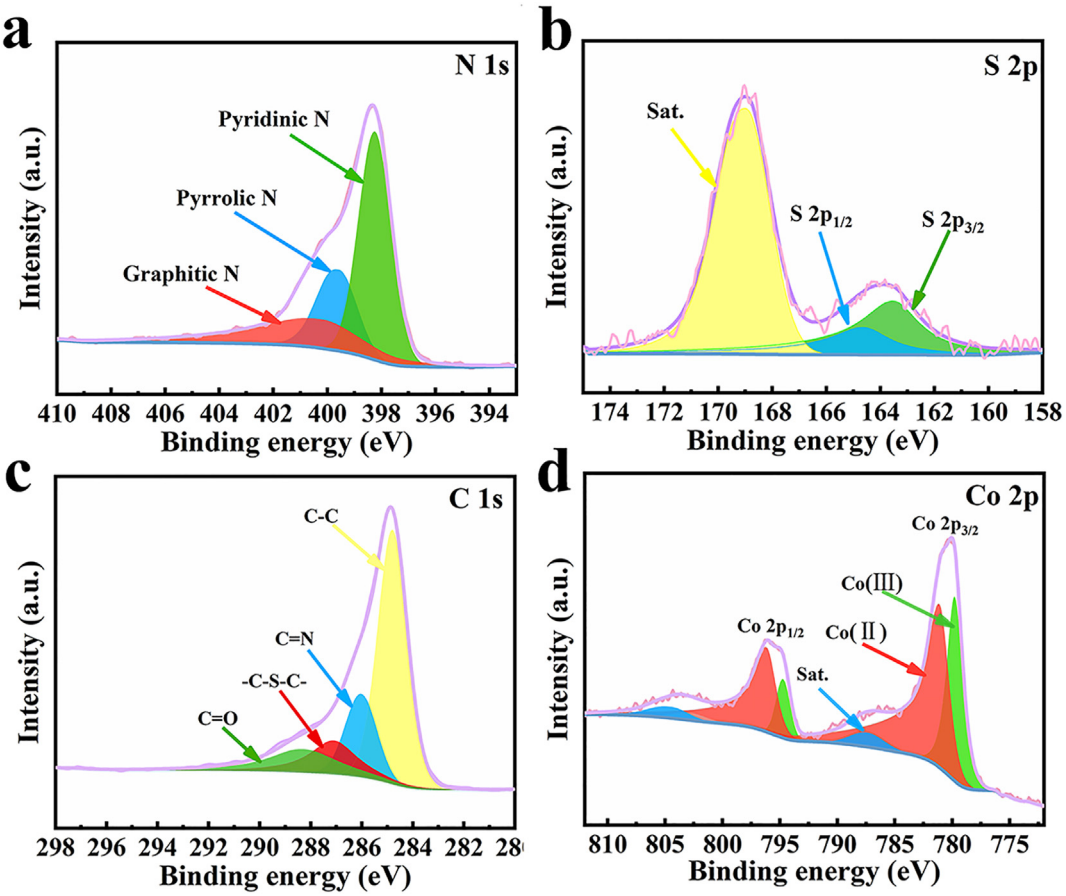

Fig. 5. The XPS spectra of the NSC/$Co_{1-x}S$: (a) N 1s; (b) S 2p; (c) C 1s and (d) Co 2p.

[35]. The diffraction peaks for NSC/$Co_{1-x}S$ were centered at 30.5, 35.2, 46.8 and 54.3° and ascribed to the (100), (101), (102) and (110) crystal planes, which were well matched with the standard PDF card (PDF # 42-0826).

Raman spectroscopic analysis revealed two characteristic peaks at 1334 cm^{-1} (D band) and 1570 cm^{-1} (G band) for both NSC and NSC/$Co_{1-x}S$ (Fig. 3b). Generally speaking, the D band is characteristic of disordered carbon or graphite structural defects, whereas the G band is associated with the level of graphitization [36]. The peak intensity ratios for the D-G band (I_D/I_G) of NSC and NSC/$Co_{1-x}S$ were 1.41 and 1.34, respectively, implying an abundance of defects in the porous structure [37]. The slightly lower I_D/I_G value for NSC/$Co_{1-x}S$ might indicate that graphitization was reduced by doping sulfur cobalt in the pyrolysis process [35]. N_2-adsorption measurements (Fig. 4c) determined that the specific surface areas of NSC/$Co_{1-x}S$ and NSC were 18.47 and 31.52 $m^2\ g^{-1}$, respectively, and a dominant pore sizes of ~7–9 nm (inset of Fig. 4c) attributable to the mesoporous structure. These observations reveal that the Co-S nanoparticles were incorporated into the pores of the carbon layers. The electron spin resonance (ESR) signal at g = 2.003 was indexed to S vacancies with the NSC/$Co_{1-x}S$ structure (Fig. 4d) [38], providing compelling evidence for the existence of S vacancies on the surface of the fabricated nanocomposite.

Elemental composition and atomic configuration information for the NSC/$Co_{1-x}S$ nanocomposite were assessed by XPS. Concentrations of N, S, C and Co in NSC/$Co_{1-x}S$ were 20.6%, 4.15%, 68.5% and 6.81% respectively, demonstrating the incorporation of N and S into the nanocomposite structure (Fig. S4). Furthermore, the single overall peak and three deconvoluted peaks in the high resolution N 1s spectrum provide additional documentation for the existence of N in the nanocomposite (Fig. 5a).

XPS peaks centered on the binding energies of 398.2, 399.6 and 400.0 eV were ascribed to pyridinic, pyrrolic and graphitic N, respectively (Fig. 5a) [39]. The N-doping was intended to increase the electron transfer speed of the NSC/$Co_{1-x}S$ nanocomposite, thereby improving the catalytic performance [40]. Meanwhile, the S 2p XPS spectrum contained peaks at 163.6 and 164.8 eV assigned to C-S $2p_{3/2}$ and $2p_{1/2}$, respectively, and another peak at 169.0 eV denoted as a satellite signal (Fig. 5b) [42]. These findings document the existence of S atoms in the composite material. The deconvolution of the C 1s XPS spectrum yielded four peaks at 284.7, 286.1, 287.1 and 288.2 eV, corresponding to C–C, C=N, -C-S-C and C=O groups, respectively (Fig. 5c) [41]. The formation of C=N and -C-S-C- moieties further demonstrate that N and S atoms were successfully doped into the carbon matrix. Finally, the Co 2p spectra displayed two broad peaks centered at 780.2 and 795.8 eV, which were ascribed to Co $2p_{3/2}$ and Co $2p_{1/2}$, respectively (Fig. 5d) [44,45]. The Co $2p_{3/2}$ peak was further deconvoluted into two peaks at 779.8 eV and 781.2 eV, assigned to Co(III) and Co(II) [49], respectively. Similarly, the Co $2p_{1/2}$ peak was deconvoluted into two peaks, corresponding to Co(III) at 794.8 eV and Co(II) at 796.5 eV. These results confirming the co-existence of Co(III) and Co(II) are consistent with the Co valence state of $Co_{1-x}S$, and thus the interconversion between Co(III) and Co (II) can significantly improve the catalytic activity of the fabricated NSC/$Co_{1-x}S$ nanocomposite [52,53].

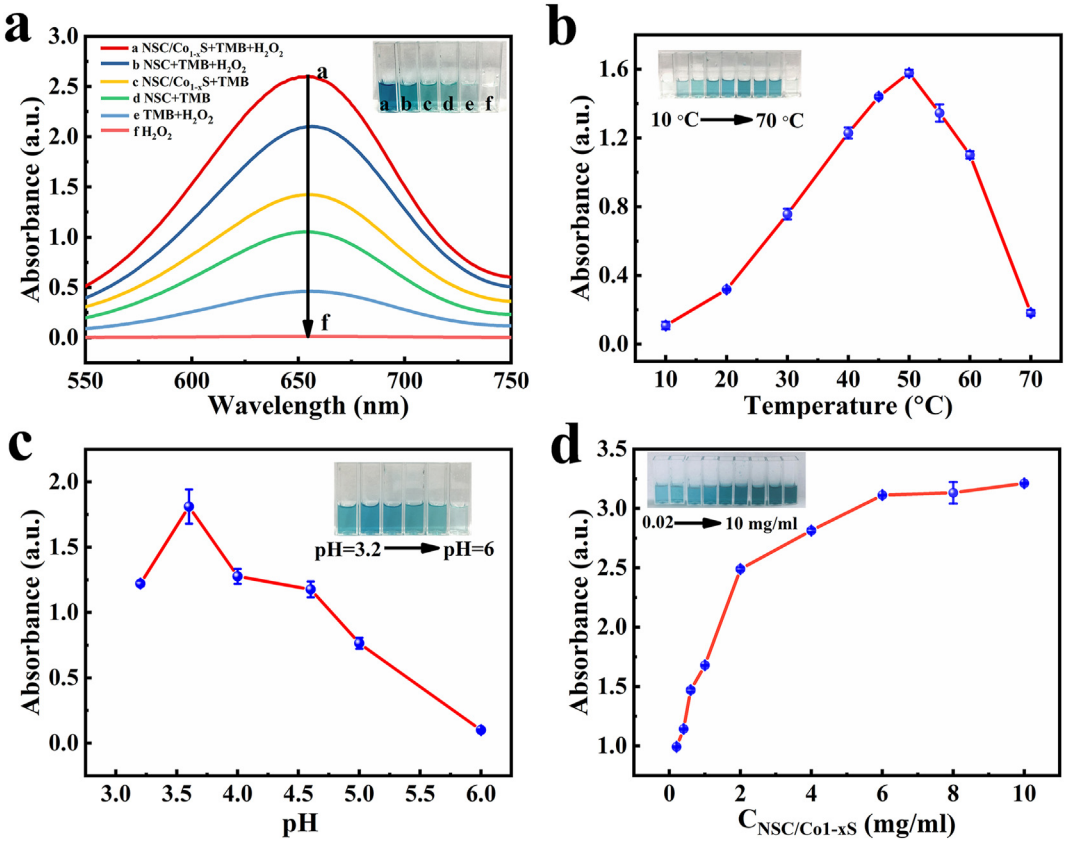

Fig. 6. (a) UV–vis absorption spectra in different systems. The effects of reaction conditions on the enzymatic-like activity of NSC/$Co_{1-x}S$: (b) temperature; (c) pH; and (d) NSC/$Co_{1-x}S$ concentration.

3.2. Enzymatic activity of the NSC/$Co_{1-x}S$ nanocomposites

Six different experiments were designed to examine the peroxidase-like activity of NSC/$Co_{1-x}S$ using TMB as a chromogenic substrate (Fig. 6a). The NSC/$Co_{1-x}S$ + H_2O_2+TMB treatment displayed the strongest 652-nm absorbance (up to ~2.50), followed by the NSC + H_2O_2+TMB treatment (~2.0). In sharp contrast, almost no 652-nm absorbance developed in the H_2O_2 treatment, but rather it retained its white color. The solution color turned blue to variable extents in the other five treatments (NSC/$Co_{1-x}S$ + H_2O_2+TMB, NSC + H_2O_2+TMB, NSC/$Co_{1-x}S$ + TMB, NSC + TMB and H_2O_2+TMB). The TMB + H_2O_2 system also exhibited a relatively weak 652-nm absorption (OD ~0.4), which may result from decomposition of a small amount of H_2O_2. Importantly, these data offer strong evidence that the NSC/$Co_{1-x}S$ system possesses strong peroxidase-mimetic activity.

To evaluate whether or not the NSC/$Co_{1-x}S$ nanocomposite possesses oxidase-like activity, the color change of solutions was observed in the presence of NSC/$Co_{1-x}S$ and absence of H_2O_2 under an O_2 or N_2 gas atmosphere. A bright blue color was observed in the presence of O_2, whereas only a weak blue color developed in the presence of N_2 (Fig. S5). Building upon the above data, we posit that when $Co_{1-x}S$ nanoparticles are anchored onto the surface of the NSC, a synergistic catalysis effect occurs in the NSC/$Co_{1-x}S$ nanocomposite. Notably, the NSC/$Co_{1-x}S$ nanoenzyme possessed both peroxidase-like and oxidase-like activities.

Activity of the nanoenzyme is closely related to the experimental conditions, and thus three key variables were selected for optimization in this investigation: temperature, pH and NSC/$Co_{1-x}S$ dosage. As the temperature increased from 10 to 50 °C, the 652-nm ODs of the NSC/$Co_{1-x}S$ system gradually increased from 0.12 to 1.58. However, with a further increase of temperature from 50 to 70 °C, the 652-nm absorbance was sharply reduced to 0.18 (Fig. 6b). We ascribe the decrease in OD at higher temperatures to a destabilization of the nanosheets at higher temperatures. With respect to solution pH, the ODs prominently increased from 1.25 to 1.59 as pH increased from 3.2 to 3.6, followed by a large decrease as the solution pH increased from 3.6 to 6.0 (Fig. 6c). Because aqueous solutions of H_2O_2 are weakly acidic, the increasing pH promotes the decomposition of H_2O_2 leading to a decrease in oxidation capacity. When the concentration of NSC/$Co_{1-x}S$ increased from 0 to 6.0 mg/mL, the ODs monotonically increased from ~1.0 to ~3.1. At higher NSC/$Co_{1-x}S$ concentrations (6.0–10.0 mg/mL), the 652-nm absorbance remained nearly unchanged (Fig. 6d). This suggests that catalytic effect of the nanozyme reaches a point beyond which higher dosages will not elicit a greater response due to complete substrate consumption [51]. Further, in UV detection systems, excessive OD values (>2.0) lead to a sharp decline in the responsivity of color recognition due to absorbance saturation. Therefore, we chose 1.0 mg/mL as the appropriate concentration for the NSC/$Co_{1-x}S$ nanocomposite. In summary, the optimized analytical conditions were set to a temperature of 50 °C, initial pH of 3.6 and a NSC/$Co_{1-x}S$ concentration of 1.0 mg/mL.

Under optimized conditions, we investigated the steady-state kinetic performance of the NSC/$Co_{1-x}S$ nanoenzyme with fortified levels of TMB (0.2–2.0 mM) and H_2O_2 (0.1–1.5 mM). The Michaelis-Menten model curves for the NSC/$Co_{1-x}S$ system are shown in Fig. 6a and b. The Michaelis constant (K_m) and maximum reaction velocity (V_{max}) were calculated based on Lineweaver-Burk plots (Fig. 7c and d). The K_m values for the NSC/$Co_{1-x}S$ system were 2.98

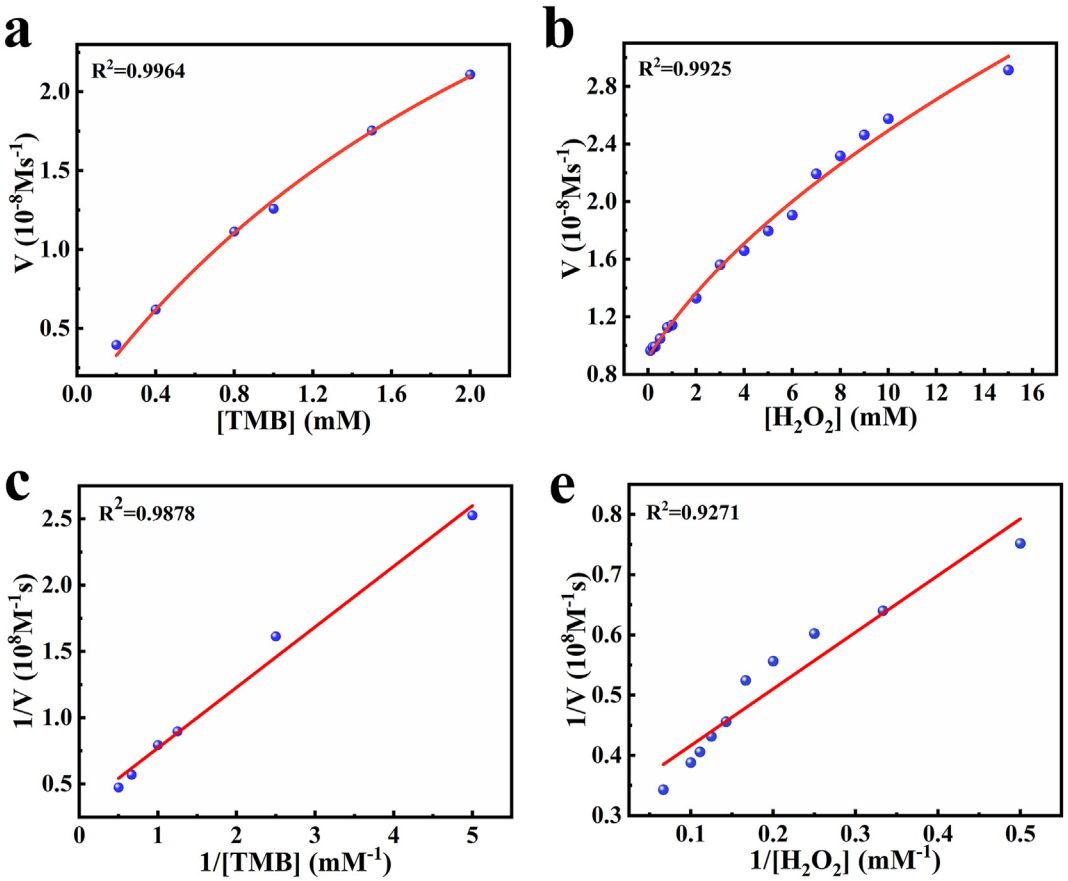

Fig. 7. Steady-state kinetics assays of NSC/$Co_{1-x}S$ by varying concentrations of (a) TMB and (b) H_2O_2; and (c, d) corresponding Lineweaver-Burk plots.

Table 1
Typical Michaelis-Menten constants for H_2O_2 and TMB substrates and their comparisons with HRP and other previously reported nanozymes.

Catalyst	Substrate	K_m (mM)	References
HRP	TMB	0.434	[48]
	H_2O_2	3.70	
Fe_3O_4	TMB	0.098	[48]
	H_2O_2	154	
Cu-N-C	TMB	3.76	[49]
	H_2O_2	19.94	
Co_3O_4	TMB	0.021	[50]
	H_2O_2	214	
Co_4N	TMB	0.243	[51]
	H_2O_2	2.95	
NSP-CQDs	TMB	0.47	[52]
	H_2O_2	32.61	
NSC/$Co_{1-x}S$	TMB	2.98	This work
	H_2O_2	2.92	

for TMB and 2.92 for H_2O_2. A smaller K_m value indicates a greater affinity for the substrate [52–56]. Accordingly, it can be concluded that the NSC/$Co_{1-x}S$ system has good catalytic performance, with H_2O_2 demonstrating a somewhat higher performance level (Table 1).

3.3. Catalytic mechanisms comprising the NSC/$Co_{1-x}S$ system

To elucidate the mechanisms involved in the NSC/$Co_{1-x}S$ catalytic performance, three ROS species (h^+, •OH and $•O_2^-$) were captured by their respective scavengers (EDTA, IPA and PBQ; Fig. 8a). In this approach, the response signal will decreased if the ROS species responsible for the catalytic reaction is captured by the scavenger. Most notably, the addition of the EDTA scavenger for h^+ resulted in a prominent reduction in the 652-nm OD indicating that h^+ played an important role in the catalytic reaction. After adding PBQ, the 652-nm OD dropped slightly, suggesting that some $•O_2^-$ was involved in the catalytic system. Finally, the presence of IPA had no significant effect on the 652-nm OD, demonstrating that •OH did not play an important role in the catalytic process.

Further, EPR analyses were carried out to deduce the possible existence of free radicals in the NSC/$Co_{1-x}S$ system (Fig. 8b–d). The characteristic signals for h^+, •OH and $•O_2^-$ were all detected demonstrating that the NSC/$Co_{1-x}S$ nanoenzyme in capable of catalyzing H_2O_2 to generate h^+, •OH and $•O_2^-$. The signal intensity for h^+ was the strongest, followed by $•O_2^-$ and •OH, consistent with the efficacy pattern acquired by the ROS scavenger assessments. Owing to the multiple valence states of Co in the NSC/$Co_{1-x}S$ nanocomposite, electronic transfer is facilitated, thereby improving the oxidation-reduction ability and promoting the catalytic process.

The absence of an electron in the bond between Co(II) and Co(III) creates a hole, which corresponds to the presence of the h^+ signal (Fig. 8b). Under acidic conditions, O_2 is converted to $•O_2^-$, and TMB is oxidized to oxTMB [34], which is consistent with the EPR results (Fig. 8c). As depicted in Fig. 6d, the characteristic signals for •OH were detected, which provides compelling evidence that the NSC/$Co_{1-x}S$ nanoenzyme catalyzes H_2O_2 to generate •OH. Hence, we posit the mechanist pathway for generation of •OH and $•O_2^-$ by NSC/$Co_{1-x}S$ with enzyme-like activities in Fig. 8e. Taken together, these findings infer that the NSC/$Co_{1-x}S$ not only exhibits superior peroxidase-like activity, but also displays potential oxidase-mimetic properties.

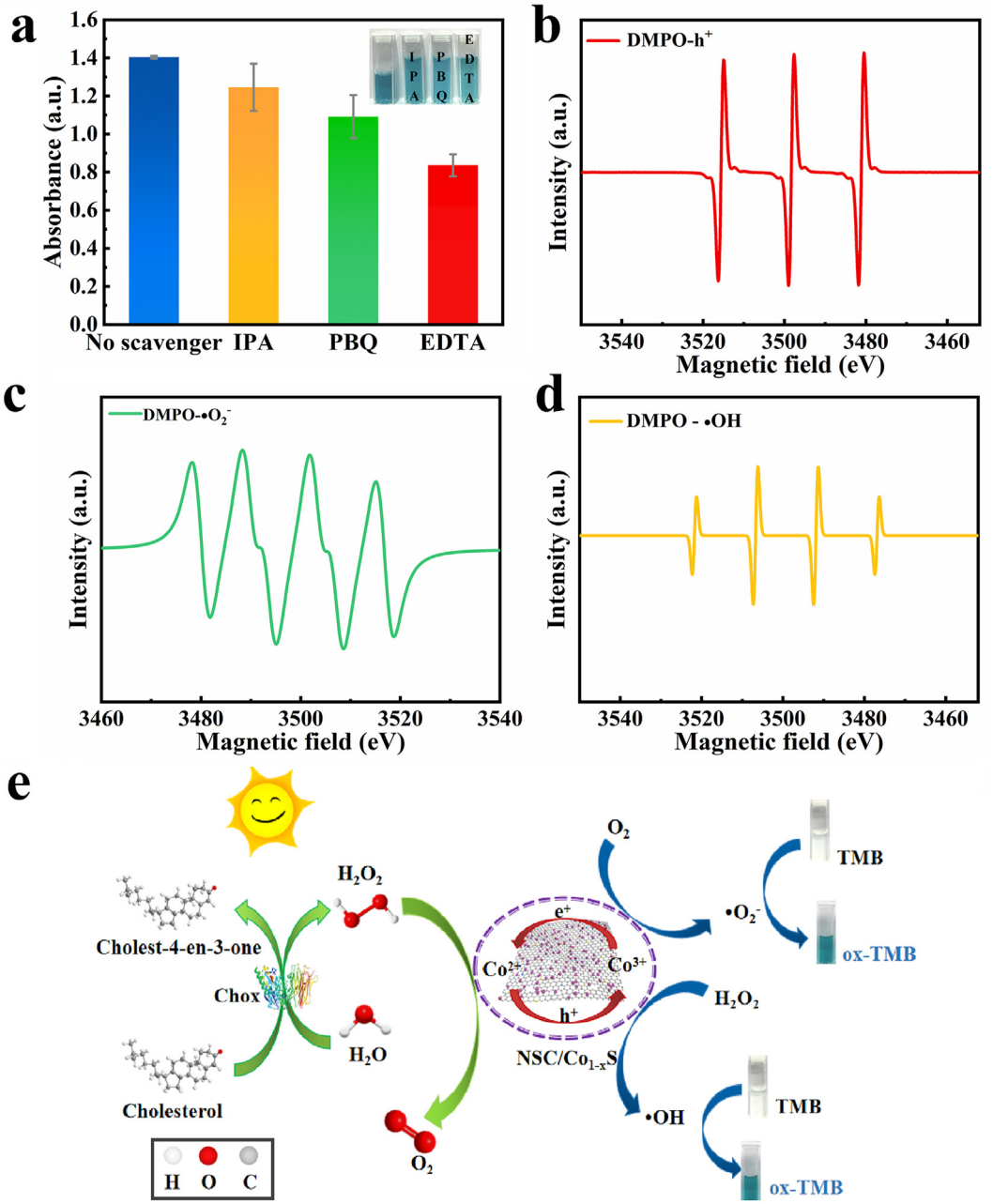

Fig. 8. (a) Effects of various active scavengers during the catalysis of TMB with the aid of NSC/$Co_{1-x}S$; (b, c and d) EPR spectra of NSC/$Co_{1-x}S$; and (e) Possible mechanism for peroxidase-like activity and oxidase-like activity of NSC/$Co_{1-x}S$.

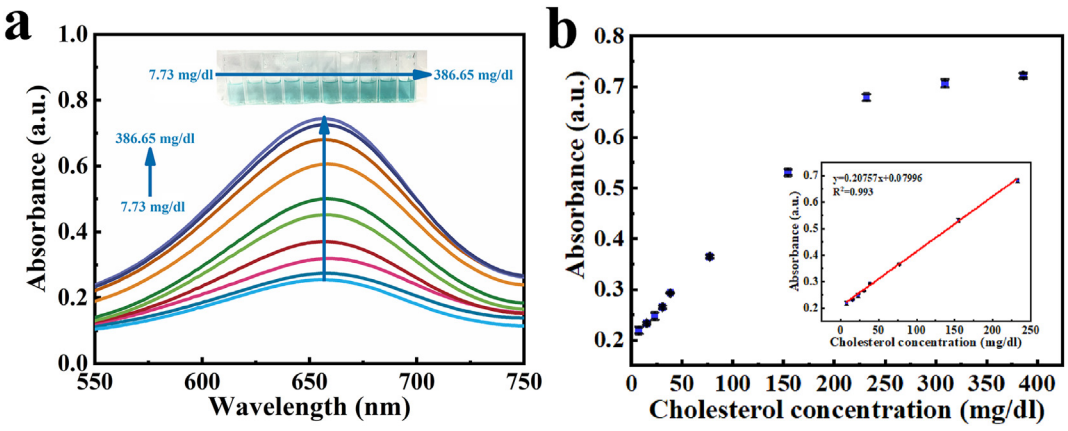

Fig. 9. (a) UV–vis absorption spectra of cholesterol with different concentrations; (b) Plots of absorbance at 652 nm versus cholesterol concentration. Inset: magnification of the plot in the range 7.73–116.00 mg/dl.

Table 2
Comparison of nanomaterial-based detection methods for Cholesterol detection.

Materials	LRs (mg/dl)	LODs (mg/dl)	Methods	Smartphone-based assay	Refs.
Au/CdS QDs/TNTs	0.93–46.40	0.46	Electrochemistry	No	[55]
NG/CIS/ZnS	12.06–193.33	8.58	Chemiluminescence	No	[56]
CuO:GNS	3.87–30.93	3.02	Colorimetry	No	[57]
N-CDs	96.67–289.99	26.29	Colorimetry	No	[20]
AgNPs + ChO_x	3.87–58.00	1.55	Colorimetry	No	[58]
$Cu_2(OH)_3Cl$-CeO_2	3.87–77.33	1.93	Colorimetry	No	[59]
Standard test strips	140–400	Unknown	Colorimetry	Yes	[12]
PPy NPs	0–3.87	0.13	Colorimetry	Yes	[13]
NSC/$Co_{1-x}S$	7.73–231.99	1.93	Colorimetry	Yes	This work

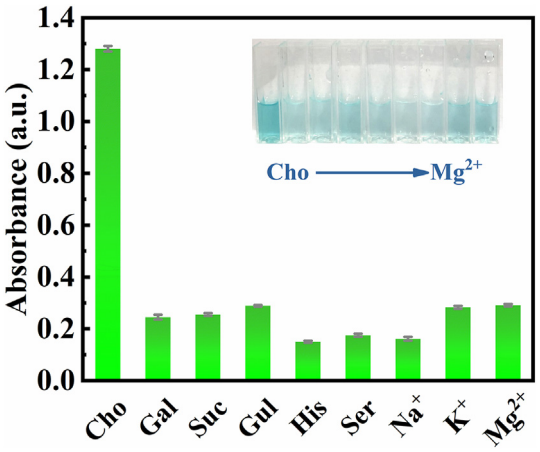

Fig. 10. The selectivity of the NSC/$Co_{1-x}S$ towards cholesterol (1.0 mM) and interferences (10 mM).

3.4. Application as a colorimetric assay for cholesterol

By employing the NSC/$Co_{1-x}S$ nanocomposite as an effective mimetic enzyme, a colorimetric biosensor was developed to quantify cholesterol through reaction with its oxidase. As detailed in Fig. 9a and b, the linear range (LR) and limit of detection (LOD) for cholesterol were 7.73–386.65 mg/dl and 1.93 mg/dl, respectively. These performance metrics were compared to several cholesterol assays reported in the literature, such as electrochemical, chemiluminescent and colorimetric methods [22,57–61]. Although electrochemical methods have a lower LOD on the basis of Au/CdS (0.46 mg/dl) [57], this method has disadvantages arising from high energy consumption and low current efficiency. The chemiluminescence approaches, such as the NG/CIS/ZnS (LR = 11.98–193.33 mg/dl, LOD = 8.51 mg/dl) [58] have a wide linear range, but poor specificity for target analytes. As summarized in Table 2, the NSC/$Co_{1-x}S$ nanoenzymatic biosensor achieves a lower or comparable LOD (1.93 mg/dl) than those of the CuO:GNS. 3.02 mg/dl) [59], N-CDs (26.29 mg/dl) [22], AgNPs + ChO_x (1.55 mg/dl) [60] and $Cu_2(OH)_3Cl$-CeO_2 (1.93 mg/dl) [61]. For the visual detection using a smartphone, the previous literature reported the quantative detection of cholesterol in the range of 140–400 mg/dl, which used the standard test strips combined with mobile-phone imaging [12]. However, the above approach offered too high detection limit to realize trace-level detection of cholesterol in blood samples or other matrices. Additionally, the reported PPy NPs could realize the visual detection of total cholesterol based on a smartphone, with a linear range of 0.39–3.87 mg/dl and a detection limit of 0.14 mg/dl [13], but our proposed methodology supplied a broader detection range (7.73–231.99 mg/dl) as compared to PPy NPs-based visual detection. As for traditional cholesterol detection, it is generally measured by drawing peripheral venous blood in hospital, and then subjected to a fully automatic biochemical instrument analysis. The price of a biochemical instrument is more expensive, and the patients also need to pay for the test. With regard to the kit detection, it also requires to purchase an assay kit and use a microplate reader to realize cholesterol detection. However, the newly developed method can quantify human serum cholesterol value only through a mobile phone app without the need for a specific analytical instrument, thereby reducing the test cost. As such, these comparative performance metrics demonstrate that the as-constructed nanoenzymic biosensor is conducive to practical applications in the analytical field of biomolecules.

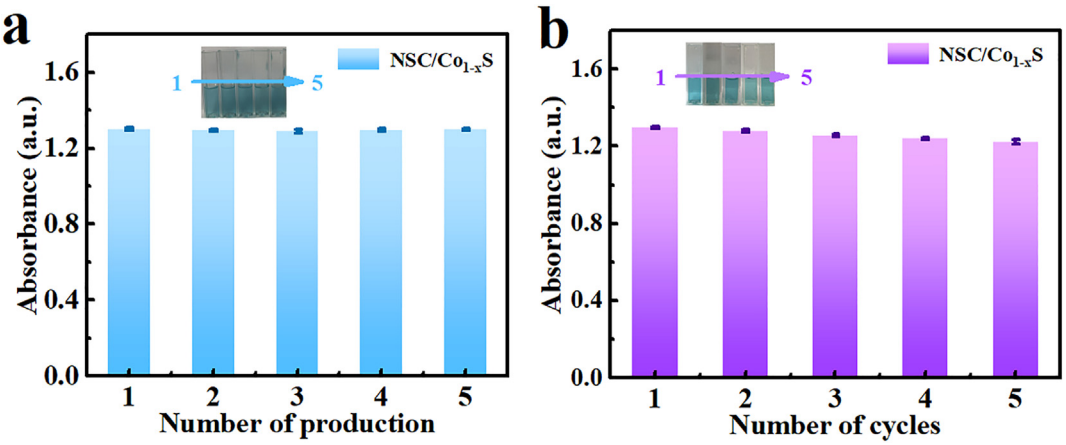

Fig. 11. (a) Repeatability and (b) reusability in cholesterol detection using the NSC/$Co_{1-x}S$.

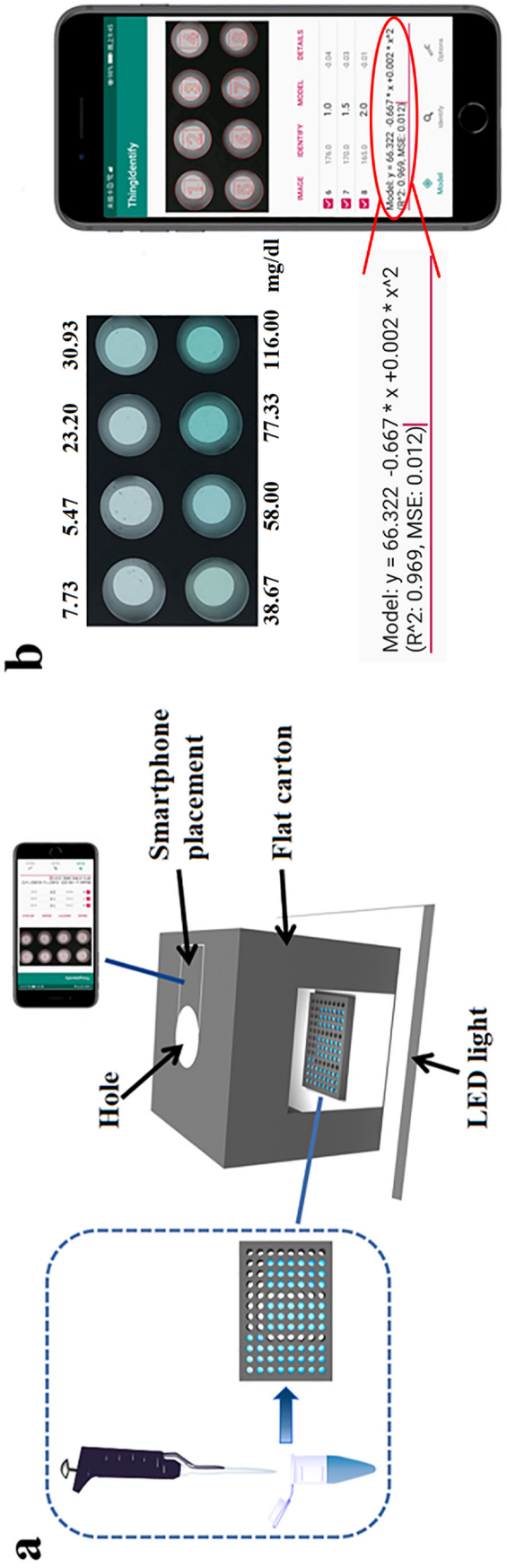

Fig. 12. (a) Simple device for detecting serum cholesterol concentrations using smartphone; and (b) Regression equation between absorbance and cholesterol concentrations (7.73–116.00 mg/dl).

3.5. Selectivity/interference constraints of the NSC/$Co_{1-x}S$-based colorimetric method for cholesterol quantification

To assess the selectivity and potential interference effects of the new developed colorimetric method, we added 10 mM of monosaccharides, amino acids and metal ions to the NSC/$Co_{1-x}S$ + TMB + H_2O_2 reaction system. The fortification levels for the interfering compounds/ions were set at 10 times higher than the cholesterol concentration (1.0 mM). The 652-nm ODs originating from the interfering solutes ranged from 0.15 to 0.30, compared to a value of ~1.1 for cholesterol with no interfering solutes (Fig. 10). This comparison suggests that interference effects from macromolecules and ions are generally low, even at high concentrations of the interfering solutes. Consequently, it can be posited that the newly developed colorimetric detection platform based on the NSC/$Co_{1-x}S$ nanoenzyme has a good selectivity/low interference potential for cholesterol analysis.

3.6. Repeatability and reusability of the NSC/$Co_{1-x}S$ nanocomposites

The 652-nm ODs were determined based on the NSC/$Co_{1-x}S$ nanocomposites from different synthetic batches under the same conditions (Fig. 10a). In the presence of cholesterol (1 mM), the nanocomposites from 5 batches gave the similar absorption values, demonstrating that the as-fabricated material had good reproducibility. The reusability of the NSC/$Co_{1-x}S$ nanozyme was monitored by examining its catalytic activity in 5 consecutive cycles for oxidizing colorless TMB into blue TMBox in the presence of cholesterol (1 mM) (Fig. 10b). It can be seen from Fig. 10b that the 652-nm ODs decreased slightly (<7.0%) after 5 cycles, which could be explained by the slight dissolution of metal ions in the reaction system [63]. These data and phenomena provide compelling evidence that the NSC/$Co_{1-x}S$ nanocomposite can be reutilized at least five times with a minor loss in its catalytic activity.

3.7. Total cholesterol assay in human serum by a smartphone APP

After optimizing the key parameters and investigating the analytical performance of this novel colorimetric method, a smartphone-based colorimetric application (app) was developed to quantitatively determine cholesterol concentrations in human serum. As displayed on the phone screen in Fig. 10a, the color intensities after catalytic reaction increased monotonically with increasing cholesterol concentrations (Fig. 11b). A calibration curve was generated by plotting the color gray values of the reacted solution versus the corresponding cholesterol concentrations. The gray value was linearly dependent on the cholesterol concentration across the range of 7.73–116.00 mg/dl (Fig. 11b). The resultant regression equation was $Y = 66.3\text{-}0.667X\text{+}0.002X^2$ ($R^2 = 0.969$), where X and Y are the reciprocal of the color gray value and the cholesterol concentration, respectively. The LOD for cholesterol offered by the app was 2.51 mg/dl (LOD = 3 s/k). After the NSC/$Co_{1-x}S$-based catalytic colorimetric reaction, the cholesterol concentration in serum was automatically detected through the "Thing Identify" software installed on the smartphone (Fig. 10a). As summarized in Table 3, the cholesterol concentrations detected by the APP were comparable with test results using a standard cholesterol test kit (Fig. S6). Relative recoveries (RRs) for cholesterol were in the range of 93.6–104.1% with RSDs of 1.7–4.7% (Table 3). These performance metrics demonstrate that the APP colorimetric method is convenient, low cost, rapid, simple and accurate, thereby offering several promising applications in point-of-care diagnosis (Fig. 12).

Table 3
Total cholesterol concentrations detected in human serum samples.

Human serum samples	Total cholesterol Assay kit (mg/dl)	Colorimetric results (mg/dl)	RSDs (%, n = 3)	Recovery rate (%)	APP results (mg/dl)	RSDs (%, n = 3)	Recovery rate (%)
1	136.87	129.07	1.3	94.3	133.78	2.2	97.7
2	165.49	156.98	2.1	94.8	172.28	1.7	104.1
3	148.47	141.13	2.2	95.0	138.97	3.9	93.6
4	146.54	148.86	3.5	101.6	139.21	4.7	95.0
5	155.05	168.07	1.6	108.4	158.15	2.9	102.0
6	207.24	204.92	1.8	98.9	203.72	3.7	98.3

4. Conclusions

The novel NSC/$Co_{1-x}S$ nanocomposite developed in this study exhibited excellent peroxidase-like and oxidase-mimetic dual-enzyme activities that catalyzed the oxidation of the chromogenic substrate TMB producing a blue color. The strong catalytic performance of NSC/$Co_{1-x}S$ resulted from the formation of ROS ($\bullet O_2^-$, h^+, $\bullet OH$), and the synergistic effect between the N, S co-doped carbon aerogel and Co-S nanoparticles having abundant S vacancies. By combining the dual-enzyme activities of NSC/$Co_{1-x}S$ with the cascade reaction of cholesterol oxidase, a visual colorimetric sensing platform with high selectivity/sensitivity was constructed for cholesterol assay. Based on the colorimetric assay and "Thing Identify" app installed on a smartphone, this NSC/$Co_{1-x}S$-based colorimetric method achieved LODs of 7.73–231.99 mg/dl in human serum. As compared to standard cholesterol test kits, relative recoveries were 93.6–104.1% with RSDs <5.0%. These analytical metrics confirm that the NSC/$Co_{1-x}S$ nanozyme-based colorimetric approach can meet the stringent requirements for point-of-use cholesterol assay in human serum samples. Therefore, this method makes it possible for medical staff to in-situ analyze blood cholesterol through a mobile app and integrates the nanomaterial into a test strip to realize point-of-care diagnosis.

CRediT authorship contribution statement

Jiani Li: Methodology, Validation, Formal analysis, Writing – original draft. **Tingting Liu:** Formal analysis, Resources, Writing – review & editing. **Randy A. Dahlgren:** Formal analysis, Writing – review & editing. **Hanzhang Ye:** Data curation, Validation. **Qi Wang:** Supervision. **Yongli Ding:** Investigation. **Ming Gao:** Project administration. **Xuedong Wang:** Conceptualization, Writing – review & editing, Funding acquisition. **Huili Wang:** Investigation, Supervision.

Declaration of competing interest

The authors declare that they have no known competing financial interests or personal relationships that could have appeared to influence the work reported in this paper.

Acknowledgement

This work was jointly supported by the National Science Foundation of China (22076134 and 21876125), Jiangsu Provincial Natural Science Foundation (BK20211338) and the Key Science & Technology Project of Suzhou City (SS202028).

Appendix A. Supplementary data

Supplementary data to this article can be found online at https://doi.org/10.1016/j.aca.2022.339703.

References

[1] N. Karanikas, C. Foster, A. Beltran Hernandez, A. Harvey, O. Targal, N. Horswill, Conventional and alternative aviation fuels: occupational exposure and health effects, J. Chem. Health Saf. 28 (2021) 159–170, https://doi.org/10.1021/acs.chas.0c00120.
[2] H. Lyu, D. Yin, B. Zhu, G. Lu, Q.Y. Liu, X. Zhang, X. Zhang, Metal-free 2(3),9(10),16(17),23(24)-octamethoxyphthalocyanine-modified uniform CoSn(OH)$_6$ nanocubes: enhanced peroxidase-like activity, catalytic mechanism, and fast colorimetric sensing for cholesterol, ACS Sustain. Chem. Eng. 8 (2020) 9404–9414, https://doi.org/10.1021/acssuschemeng.0c02151.
[3] Y. Li, Z. Kang, L. Kong, H. Shi, Y. Zhang, M. Cui, D.P. Yang, MXene-Ti_3C_2/CuS nanocomposites: enhanced peroxidase-like activity and sensitive colorimetric cholesterol detection, Mater. Sci. Eng. C 104 (2019), 110000, https://doi.org/10.1016/j.msec.2019.110000.
[4] M. Zhao, M. Bergaentzlé, A. Flieller, E. Marchioni, Development and validation of an ultra-high performance liquid chromatography-high resolution mass spectrometry method for simultaneous quantification of cyanogenic glycosides and secoisolariciresinol diglucoside in flaxseed (Linum usitatissimum L.), J. Chromatogr., A 1601 (2019) 214–223, https://doi.org/10.1016/j.chroma.2019.04.072.
[5] Y. He, N. Li, W. Li, X. Zhang, X. Zhang, Z. Liu, Q. Liu, 5,10,15,20-tetrakis (4-carboxylphenyl) porphyrin functionalized $NiCo_2S_4$ yolk-shell nanospheres: excellent peroxidase-like activity, catalytic mechanism and fast cascade colorimetric biosensor for cholesterol, Sensor. Actuator. B Chem. 326 (2021), 128850, https://doi.org/10.1016/j.snb.2020.128850.
[6] H. Peng, J. Zhang, C. Zeng, C. Zhou, Q. Li, N. Lu, L. Wang, One-dimensional synergistic core-Shell nanozymes with superior peroxidase-like activity for ultrasensitive colorimetric detection of blood cholesterol, ACS Appl. Bio Mater. 3 (2020) 5111–5119, https://doi.org/10.1021/acsabm.0c00588.
[7] G.B. Hu, C.Y. Xiong, W. Bin Liang, X.S. Zeng, H.L. Xu, Y. Yang, L.Y. Yao, R. Yuan, D.R. Xiao, Highly stable mesoporous luminescence-functionalized MOF with excellent electrochemiluminescence property for ultrasensitive immunosensor construction, ACS Appl. Mater. Interfaces 10 (2018) 15913–15919, https://doi.org/10.1021/acsami.8b05038.
[8] D.P. Yang, W. Guo, Z. Cai, Y. Chen, X. He, C. Huang, J. Zhuang, N. Jia, Highly sensitive electrochemiluminescence biosensor for cholesterol detection based on AgNPs-BSA-MnO_2 nanosheets with superior biocompatibility and synergistic catalytic activity, Sensor. Actuator. B Chem. 260 (2018) 642–649, https://doi.org/10.1016/j.snb.2018.01.096.
[9] H. Kim, H. Kim, S. Kumar, D.W. Kang, H. Jo, H. Jo, J.H. Park, J.H. Park, Affinity-driven design of cargo-switching nanoparticles to leverage a cholesterol-rich microenvironment for atherosclerosis therapy, ACS Nano 14 (2020) 6519–6531, https://doi.org/10.1021/acsnano.9b08216.
[10] H. Xu, S. Zhou, D. Jiang, H.Y. Chen, Cholesterol oxidase/triton X-100 parked microelectrodes for the detection of cholesterol in plasma membrane at single cells, Anal. Chem. 90 (2018) 1054–1058, https://doi.org/10.1021/acs.analchem.7b03667.
[11] K. Liu, S. Huang, D. Fang, Electrochemical measurement of cholesterol flip-flop in plasma membrane at single cells, Anal. Chem. 92 (2020) 10961–10965, https://doi.org/10.1021/acs.analchem.0c01991.
[12] V. Oncescu, M. Mancuso, D. Erickson, Cholesterol testing on a smartphone, Lab Chip 14 (2014) 759–763, https://doi.org/10.1039/c3lc51194d.
[13] C. Hong, X. Zhang, C. Wu, Q. Chen, H. Yang, D. Yang, Z. Huang, R. Cai, W. Tan, On-site colorimetric detection of cholesterol based on polypyrrole nanoparticles, ACS Appl. Mater. Interfaces 12 (2020) 54426–54432, https://doi.org/10.1021/acsami.0c15900.
[14] L. Gao, J. Zhuang, L. Nie, J. Zhang, Y. Zhang, N. Gu, T. Wang, J. Feng, D. Yang, S. Perrett, X. Yan, Intrinsic peroxidase-like activity of ferromagnetic nanoparticles, Nat. Nanotechnol. 2 (2007) 577–583, https://doi.org/10.1038/nnano.2007.260.
[15] L. Zhang, X. Hai, C. Xia, X.W. Chen, J.H. Wang, Growth of CuO nanoneedles on graphene quantum dots as peroxidase mimics for sensitive colorimetric detection of hydrogen peroxide and glucose, Sensor. Actuator. B Chem. 248 (2017) 374–384, https://doi.org/10.1016/j.snb.2017.04.011.
[16] P. Gallay, M. Eguílaz, G. Rivas, Designing electrochemical interfaces based on nanohybrids of avidin functionalized-carbon nanotubes and ruthenium nanoparticles as peroxidase-like nanozyme with supramolecular recognition properties for site-specific anchoring of biotinylated residues, Biosens.

Bioelectron. 148 (2020), 111764, https://doi.org/10.1016/j.bios.2019.111764.
[17] S.K. Pandey, S. Sachan, S.K. Singh, Electrochemically reduced graphene oxide modified with electrodeposited thionine and horseradish peroxidase for hydrogen peroxide sensing and inhibitive measurement of chromium, Mater. Sci. Energy Technol. 2 (2019) 676–686, https://doi.org/10.1016/j.mset.2019.08.001.
[18] M. Arivazhagan, G. Maduraiveeran, Ultra-fine nickel sulfide nanoclusters @ nickel sulfide microsphere as enzyme-free electrode materials for sensitive detection of lactic acid, J. Electroanal. Chem. 874 (2020), 114465, https://doi.org/10.1016/j.jelechem.2020.114465.
[19] P. Rai, V.P. Singh, J. Peralta-Videa, D.K. Tripathi, S. Sharma, F.J. Corpas, Hydrogen sulfide (H_2S) underpins the beneficial silicon effects against the copper oxide nanoparticles (CuO NPs) phytotoxicity in oryza sativa seedlings, J. Hazard Mater. (2021), 124907, https://doi.org/10.1016/j.jhazmat.2020.124907.
[20] W. Zhang, N. Li, Q. Chang, Z. Chen, S. Hu, Making a cup of carbon dots for ratiometric and colorimetric fluorescent detection of Cu^{2+} ions, Colloids Surf. A Physicochem. Eng. Asp. 586 (2020), 124233, https://doi.org/10.1016/j.colsurfa.2019.124233.
[21] R. Wang, G. Ruan, Y. Sun, D. Zhao, H. Yu, C.W. Zhang, L. Li, J. Liu, A full-wavelength coverage colorimetric sensor depending on polymer-carbon nanodots from blue to red for visual detection of nitrite via smartphone, Dyes Pigments 191 (2021), 109383, https://doi.org/10.1016/j.dyepig.2021.109383.
[22] N. Kitchawengkul, A. Prakobkij, W. Anutrasakda, N. Yodsin, S. Jungsuttiwong, S. Chunta, M. Amatatongchai, P. Jarujamrus, Mimicking peroxidase-like activity of nitrogen-doped carbon dots (N-CDs) coupled with a laminated three-dimensional microfluidic paper-based analytical device (laminated 3D-μPAD) for smart sensing of total cholesterol from whole blood, Anal. Chem. 93 (2021) 6989–6999, https://doi.org/10.1021/acs.analchem.0c05459.
[23] P. Wang, F. Wei, Z. Zhao, Y. Guo, S. Du, Z. Hao, Effect of heat treatment temperature on mechanical and tribological properties of copper impregnated carbon/carbon composite, Tribol. Int. (2021), 107209, https://doi.org/10.1016/j.triboint.2021.107209.
[24] M.H. Chiu, L.Y. Lin, Y.J. Hsiao, Improving energy storage ability of acid-treated carbon fibers via simple sonication and heat treatments for flexible supercapacitors, Energy Rep. 7 (2021) 4205–4213, https://doi.org/10.1016/j.egyr.2021.06.074.
[25] C. Xu, M. Cai, Y. Fang, X. Wang, Y. Chen, L. Dai, Enhanced performance of binary WO_3/N-doped carbon composites for the catalytic oxidation of benzyl alcohol under mild conditions, Mol. Catal. 510 (2021), 111690, https://doi.org/10.1016/j.mcat.2021.111690.
[26] S. Bao, H. Liu, H. Liang, C. Li, J. Bai, Electrospinned silk-ribbon-like carbon-doped TiO_2 ultrathin nanosheets for enhanced visible-light photocatalytic activity, Colloids Surf. A Physicochem. Eng. Asp. 616 (2021), 126289, https://doi.org/10.1016/j.colsurfa.2021.126289.
[27] A. Nsabimana, S.A. Kitte, F. Wu, L. Qi, Z. Liu, M.N. Zafar, R. Luque, G. Xu, Multifunctional magnetic Fe_3O_4/nitrogen-doped porous carbon nanocomposites for removal of dyes and sensing applications, Appl. Surf. Sci. 467–468 (2019) 89–97, https://doi.org/10.1016/j.apsusc.2018.10.119.
[28] L. Zhang, F. Fu, B. Tang, Adsorption and redox conversion behaviors of Cr(VI) on goethite/carbon microspheres and akaganeite/carbon microspheres composites, Chem. Eng. J. 356 (2019) 151–160, https://doi.org/10.1016/j.cej.2018.08.224.
[29] S. Wang, G. Zhou, J. Lv, Y. Ma, Y. Wang, C. Hu, J. Zhang, J. Yang, G. He, M. Zhang, M. Zhao, X. Chen, L. Yang, Co_9S_8/CoS@S, N co-doped porous carbon derived from MOFs as an efficient catalyst for the oxygen evolution reaction, J. Phys. Chem. Solid. 148 (2021), 109696, https://doi.org/10.1016/j.jpcs.2020.109696.
[30] W. Ding, H. Liu, W. Zhao, J. Wang, L. Zhang, Y. Yao, C. Yao, C. Song, A hybrid of FeS_2 nanoparticles encapsulated by two-dimensional carbon sheets as excellent nanozymes for colorimetric glucose detection, ACS Appl. Bio Mater. 3 (2020) 5905–5912, https://doi.org/10.1021/acsabm.0c00605.
[31] F. Nekouei, S. Nekouei, O. Jashnsaz, M. Pouzesh, Green approach for in-situ growth of highly-ordered 3D flower-like CuS hollow nanospheres decorated on nitrogen and sulfur co-doped graphene bionanocomposite with enhanced peroxidase-like catalytic activity performance for colorimetric biosensing of gluco, Mater. Sci. Eng. C 90 (2018) 576–588, https://doi.org/10.1016/j.msec.2018.05.001.
[32] Y. He, N. Li, J. Lian, Z. Yang, Z. Liu, Q. Liu, X. Zhang, X. Zhang, Colorimetric ascorbic acid sensing from a synergetic catalytic strategy based on 5,10,15,20-tetra(4-pyridyl)-21H,23H-porphyrin functionalized CuS nanohexahedrons with the enhanced peroxidase-like activity, Colloids Surf. A Physicochem. Eng. Asp. 598 (2020), 124855, https://doi.org/10.1016/j.colsurfa.2020.124855.
[33] Y. Gao, C. Jin, X. Li, K. Wu, L. Gao, X. Lyu, X. Zhang, X. Zhang, X. Luo, Q. Liu, Two-dimensional porphyrin-Co_9S_8 nanocomposites with synergistic peroxidase-like catalysis: synthesis and application toward colorimetric biosensing of H_2O_2 and glutathione, Colloids Surf. A Physicochem. Eng. Asp. 568 (2019) 248–258, https://doi.org/10.1016/j.colsurfa.2019.02.032.
[34] S.W. Lv, N. Zhao, J.M. Liu, F.E. Yang, C.Y. Li, S. Wang, Newly constructed $NiCo_2O_4$ derived from ZIF-67 with dual mimic enzyme properties for colorimetric detection of biomolecules and metal ions, ACS Appl. Mater. Interfaces (2021), https://doi.org/10.1021/acsami.1c06705.
[35] Y. Zou, Y. Gu, B. Hui, X. Yang, H. Liu, S. Chen, R. Cai, J. Sun, X. Zhang, D. Yang, Nitrogen and sulfur vacancies in carbon shell to tune charge distribution of $Co_6Ni_3S_8$ core and boost sodium storage, Adv. Energy Mater. 10 (2020) 1–10, https://doi.org/10.1002/aenm.201904147.
[36] W. Liu, L. Chu, C. Zhang, P. Ni, Y. Jiang, B. Wang, Y. Lu, C. Chen, Hemin-assisted synthesis of peroxidase-like Fe-N-C nanozymes for detection of ascorbic acid-generating bio-enzymes, Chem. Eng. J. 415 (2021), 128876, https://doi.org/10.1016/j.cej.2021.128876.
[37] W. Wei, F. Wang, J. Yang, J. Zou, J. Li, K. Shi, A superior potassium-ion anode material from pitch-based activated carbon fibers with hierarchical pore structure prepared by metal catalytic activation, ACS Appl. Mater. Interfaces 13 (2021) 6557–6565, https://doi.org/10.1021/acsami.0c22184.
[38] W. Liu, J. Tian, C. Mao, Z. Wang, J. Liu, R.A. Dahlgren, L. Zhang, X. Wang, Sulfur Vacancy Promoted Peroxidase-like Activity of Magnetic Greigite (Fe_3S_4) for Colorimetric Detection of Serum Glucose, Elsevier B.V., 2020, https://doi.org/10.1016/j.aca.2020.06.056.
[39] J. Mujtaba, L. He, H. Zhu, Z. Xiao, G. Huang, A.A. Solovev, Y. Mei, Co_9S_8 nanoparticles for hydrogen evolution, ACS Appl. Nano Mater (2021) 4–13, https://doi.org/10.1021/acsanm.0c03171.
[40] A. Wang, L. Cheng, X. Shen, X. Chen, W. Zhu, W. Zhao, C. Lv, Porphyrin coordination polymer/$Co_{1-x}S$ composite electrocatalyst for efficient oxygen evolution reaction, Chem. Eng. J. 400 (2020), 125975, https://doi.org/10.1016/j.cej.2020.125975.
[41] Y. Yu, Z. Zhan, P. Tang, Q. Xu, Q. Fan, W. Wang, K. Shen, Promoting polysulfide redox kinetics by Co_9S_8 nanoparticle-embedded in N-doped carbon nanotube hollow polyhedron for lithium sulfur batteries, J. Alloys Compd. 869 (2021), https://doi.org/10.1016/j.jallcom.2021.159306.
[42] X. Xu, T. Wei, R. Xiong, Z. Zhang, X. Zhang, S. Qiao, Q. Li, Y. Hu, Ammonium fluoride regulated $CoMoS_4$-derived Co_9S_8@MoS_2 composite for high-performance hybrid supercapacitor, Surf. Coating. Technol. 413 (2021), 127085, https://doi.org/10.1016/j.surfcoat.2021.127085.
[44] C. Feng, Z. Chen, J. Jing, M. Sun, J. Han, K. Fang, W. Li, Synergistic effect of hierarchical structure and Z-scheme heterojunction constructed by CdS nanoparticles and nanoflower-structured Co_9S_8 with significantly enhanced photocatalytic hydrogen production performance, J. Photochem. Photobiol. Chem. 409 (2021), 113160, https://doi.org/10.1016/j.jphotochem.2021.113160.
[45] L. Zheng, W. Ye, P. Yang, J. Song, X. Shi, H. Zheng, Manganese doping to boost the capacitance performance of hierarchical Co_9S_8@$Co(OH)_2$ nanosheet arrays, Green Energy Environ. (2021), https://doi.org/10.1016/j.gee.2021.02.002, 0–8.
[48] Y. Ding, Q. Xue, Q.L. Hong, F.M. Li, Y.C. Jiang, S.N. Li, Y. Chen, Hydrogen and potassium acetate co-production from electrochemical reforming of ethanol at ultrathin cobalt sulfide nanosheets on nickel foam, ACS Appl. Mater. Interfaces 13 (2021) 4026–4033, https://doi.org/10.1021/acsami.0c20554.
[49] D. He, X. Wu, W. Liu, C. Lei, C. Yu, G. Zheng, J. Pan, L. Lei, X. Zhang, $Co_{1-x}S$ embedded in porous carbon derived from metal organic framework as a highly efficient electrocatalyst for oxygen evolution reaction, Chin. Chem. Lett. 30 (2019) 229–233, https://doi.org/10.1016/j.cclet.2018.03.020.
[50] Y. Liu, J. Zhang, Y. Li, G. Yuan, X. Niu, X. Zhang, Q. Wang, Self-templated synthesis of $Co_{1-x}S$ porous hexagonal microplates for efficient electrocatalytic oxygen evolution, Chemelectrochem 5 (2018) 1167–1172, https://doi.org/10.1002/celc.201800026.
[51] N. Khaliq, M.A. Rasheed, M. Khan, M. Maqbool, M. Ahmad, S. Karim, A. Nisar, P. Schmuki, S.O. Cho, G. Ali, Voltage-switchable biosensor with gold nanoparticles on TiO_2 nanotubes decorated with CdS quantum dots for the detection of cholesterol and H_2O_2, ACS Appl. Mater. Interfaces (2021), https://doi.org/10.1021/acsami.0c19979.
[52] L. Su, J. Feng, X. Zhou, C. Ren, H. Li, X. Chen, Colorimetric detection of urine glucose based $ZnFe_2O_4$ magnetic nanoparticles, Anal. Chem. 84 (2012) 5753–5758, https://doi.org/10.1021/ac300939z.
[53] Y. Wu, J. Wu, L. Jiao, W. Xu, H. Wang, X. Wei, W. Gu, G. Ren, N. Zhang, Q. Zhang, L. Huang, L. Gu, C. Zhu, Cascade reaction system integrating single-atom nanozymes with abundant Cu sites for enhanced biosensing, Anal. Chem. 92 (2020) 3373–3379, https://doi.org/10.1021/acs.analchem.9b05437.
[54] J. Huo, J. Hao, J. Mu, Y. Wang, Surface modification of Co_3O_4 nanoplates as efficient peroxidase nanozymes for biosensing application, ACS Appl. Bio Mater. 4 (2021) 3443–3452, https://doi.org/10.1021/acsabm.1c00017.
[55] Y.Z. Li, T.T. Li, W. Chen, Y.Y. Song, Co_4N nanowires: noble-metal-free peroxidase mimetic with excellent salt- and temperature-resistant abilities, ACS Appl. Mater. Interfaces 9 (2017) 29881–29888, https://doi.org/10.1021/acsami.7b09861.
[56] K.M. Tripathi, H.T. Ahn, M. Chung, X.A. Le, D. Saini, A. Bhati, S.K. Sonkar, M. Il Kim, T.Y. Kim, N, S, and P-co-doped carbon quantum dots: intrinsic peroxidase activity in a wide pH range and its antibacterial applications, ACS Biomater. Sci. Eng. 6 (2020) 5527–5537, https://doi.org/10.1021/acsbiomaterials.0c00831.
[57] T. Xia, G. Liu, J. Wang, S. Hou, S. Hou, MXene-based enzymatic sensor for highly sensitive and selective detection of cholesterol, Biosens. Bioelectron. 183 (2021), 113243, https://doi.org/10.1016/j.bios.2021.113243.
[58] R. Adel, S. Ebrahim, A. Shokry, M. Soliman, M. Khalil, Nanocomposite of CuInS/ZnS and nitrogen-doped graphene quantum dots for cholesterol sensing, ACS Omega 6 (2021) 2167–2176, https://doi.org/10.1021/acsomega.0c05416.
[59] V. Sharma, S.M. Mobin, Cytocompatible peroxidase mimic CuO:Graphene nanosphere composite as colorimetric dual sensor for hydrogen peroxide and cholesterol with its logic gate implementation, Sensor. Actuator. B Chem. 240 (2017) 338–348, https://doi.org/10.1016/j.snb.2016.08.169.
[60] H.V. Tran, T.V. Nguyen, L.T.N. Nguyen, H.S. Hoang, C.D. Huynh, Silver nanoparticles as a bifunctional probe for label-free and reagentless colorimetric

hydrogen peroxide chemosensor and cholesterol biosensor, J. Sci. Adv. Mater. Dev. 5 (2020) 385–391, https://doi.org/10.1016/j.jsamd.2020.06.001.
[61] N. Wang, J. Sun, L. Chen, H. Fan, S. Ai, A $Cu_2(OH)_3Cl$-CeO_2 nanocomposite with peroxidase-like activity, and its application to the determination of hydrogen peroxide, glucose and cholesterol, Microchim. Acta 182 (2015) 1733–1738, https://doi.org/10.1007/s00604-015-1506-8.
[63] S.E. Son, P.K. Gupta, W. Hur, H.B. Lee, Y. Park, J. Park, S.N. Kim, G.H. Seong, Citric acid-functionalized rhodium-platinum nanoparticles as peroxidase mimics for determination of cholesterol, ACS Appl. Nano Mater. 4 (2021) 8282–8291, https://doi.org/10.1021/acsanm.1c01457.